Walls of orientation induced in nematic-liquid-crystal samples by inhomogeneous surfaces

L. R. Evangelista and G. Barbero*

Departamento de Física, Universidade Estadual de Maringá, 87020-900 Maringá, Paraná, Brazil

(Received 13 October 1993)

A theoretical analysis of the walls of orientation induced in nematic liquid crystal by inhomogeneous surfaces is presented. The case in which the nematic liquid crystals may be approximated by a semi-infinite medium is considered for different kinds of inhomogeneities. The same analysis is extended to a slab of nematic liquid crystal of definite thickness. The influence of the thickness of the sample on the width of the wall of orientation is evaluated in the frame of strong- and weak-anchoring situations. The threshold field for the Fréedericksz effect for nematic samples characterized by uniform easy axis but nonuniform anchoring energy on the experimental determination of the anchoring energy strength is discussed.

PACS number(s): 61.30.Gd, 61.30.Jf, 02.90.+p

I. INTRODUCTION

The elastic theory of nematic liquid crystals (NLC) has been formulated long ago by Ericksen [1] and Leslie [2], and described in many textbooks [3–5]. This theory is mainly applied to the study of one-dimensional problems, in which all the physical quantities depend only on one coordinate [6]. In this frame it is possible to describe the well known Fréedericksz transition [7] and a few other structures useful for practical applications [6]: among others, the supertwisted nematic cell [8] and the hybrid aligned nematic cell [9]. The first arrangement is very important for display applications [10]. It is relevant to a slab of NLC, in which the nematic orientation is planar on the two orienting surfaces, but the relative angle of one surface with respect to the other one is larger than $\pi/2$. The second arrangement corresponds to a NLC cell whose nematic orientation is planar on one of the surfaces (i.e., the director is parallel to the surface) and homeotropic on the other one (i.e., the director is normal to the other surface). It has been important in determining different NLC physical parameters, like the flexoelectric coefficients [11–13] or the anchoring energy [14,15].

Recently elastic theory has been applied to analyze two-dimensional periodical patterns induced by external fields [16–20], following the pioneering paper by Lonberg and Meyer [21]. However, in this paper the surface treatment was thought to be uniform. An extension of the elastic theory to two-dimensional problems has been carried out by Kléman [22] in order to describe the disclination in NLC. In his work, Kléman was mainly interested in surface defects in the absence of external fields. He analyzed, in particular, the structure and the width of the disclination walls. More recently [23–25], some attention has been given to the NLC orientation induced by surface nonhomogeneities. This has been done to im-

prove the definition of the surface energy [24] in a continuum description and to connect the anchoring energy experimentally detected with the random distribution of easy axes [25]. In this paper, the analysis of Ref. [25] is extended in order to describe walls of NLC orientation induced by a sharp variation of surface treatment. We also analyze the threshold for the Fréedericksz transition in NLC samples, for which the surface treatment is characterized by a variable anchoring energy.

Our paper is organized as follows. In Sec. II the walls of NLC orientation in semi-infinite samples are discussed. This problem is simple from an analytical point of view, but a few important conclusions may be easily derived. In Sec. III the same problem for NLC samples having the shape of a slab is considered. There the role of the thickness of the sample on the width of the walls of orientation is discussed. The possibility of experimentally detecting surface walls is analyzed too. The theoretical determination of the threshold for the Fréedericksz effect is reported in Sec. IV. There we show that the theoretical threshold is fixed by the lowest anchoring energy. However, the experimental detectability of this threshold strongly depends on the spatial extension over which this lowest anchoring energy is delocalized. The main conclusions of our paper are stressed in Sec. V.

II. SEMI-INFINITE MEDIUM

Let us consider a semi-infinite medium, limited by the (x,y) plane placed at $z=0$. The NLC medium occupies the $z>0$ half space. The NLC direction $\mathbf{n}$ is supposed to be everywhere parallel to the (x,z) plane. The tilt angle ϕ made by $\mathbf{n}$ with the z axis is considered y independent. The surface orientation imposed by the surface treatment is supposed to be of the kind

$$\Phi(x) = \begin{cases} \Phi_1, & x<0 \\ \Phi_2, & x>0, \end{cases} \tag{1}$$

and independent of the bulk NLC orientation. This is the case known as the strong-anchoring situation. The elas-

tic energy density of a NLC, in the continuum approximation is given by

$$f = \tfrac{1}{2}K(\nabla\phi)^2 , \qquad (2)$$

in the one-constant approximation. In (2), K is the Frank elastic constant. The actual $\phi(x,z)$ profile is obtained by minimizing the total elastic energy given by

$$F = \int_{-\infty}^{\infty} \int_{0}^{\infty} \tfrac{1}{2}K(\nabla\phi)^2 dx\, dz , \qquad (3)$$

per unit length along the y axis. Minimization of (3) gives, for $\phi(x,z)$,

$$\frac{\partial^2\phi}{\partial x^2} + \frac{\partial^2\phi}{\partial z^2} = 0 , \qquad (4)$$

hence $\phi(x,z)$ is a harmonic function, whose boundary conditions are given by Eq. (1). This is the well-known Dirichlet problem. Simple considerations show that the solution of (4), assuming on the border $z = 0$ the value $\Phi(x)$, is given by

$$\phi(x,z) = \frac{1}{\pi} \int_{-\infty}^{\infty} \frac{z}{z^2 + (x - x')^2} \Phi(x')dx' . \qquad (5)$$

In the event in which $\Phi(x)$ is of the kind (1), simple calculations give for $\phi(x,z)$ the expression

$$\phi(x,z) = \tfrac{1}{2}(\Phi_1 + \Phi_2) + \frac{(\Phi_2 - \Phi_1)}{\pi}\arctan\left[\frac{x}{z}\right] . \qquad (6)$$

A simple inspection shows that $\phi(x,z)$ is a harmonic function satisfying the boundary conditions (1). Figure 1(a) shows $\phi(x,z)$ vs x and z. In this case, the "wall" of nematic orientation has infinite thickness, as expected. In fact, the wall is the region in which $\phi(x,z)$ strongly differs from Φ_1 or Φ_2. For the problem we are analyzing it is defined by $\phi(x,z) = \Phi_1 + \varepsilon$, if $x < 0$, and $\phi(x,z) = \Phi_2 - \varepsilon$, if $x > 0$, where ε depends on the accuracy by means of which we want to define the nonuniform part of $\phi(x,z)$, i.e., the walls of orientation. By using Eq. (6), the above reported conditions give $x_- = -(\cot \varepsilon)z$, for $x < 0$, and $x_+ = (\cot \varepsilon)z$, for $x > 0$, for the border of the uniform distribution of $\phi(x,z)$. The thickness of the wall, defined as $x_+ - x_-$, is then $2(\cot \varepsilon)z$. It tends to infinity when $z \to \infty$, as previously stated. This is shown in Fig. 1(b), where different ε's are shown.

The elastic energy density of the distortion given by (6) is

$$f = \tfrac{1}{2}K(\nabla\phi)^2 = \tfrac{1}{2}K\left[\frac{\Phi_2 - \Phi_1}{\pi}\right]^2 \frac{1}{r^2} , \qquad (7)$$

where $r^2 = x^2 + z^2$. As is well known, f diverges near to $x = z = 0$. At this point there is a disclination which is shown in Fig. 1(c). The thickness of the wall on the surface is zero. This is due to the hypothesis of strong anchoring. Moving from the surface disclination to $z \to \infty$, the orientation wall becomes larger and larger, and the elastic energy density tends rapidly to zero

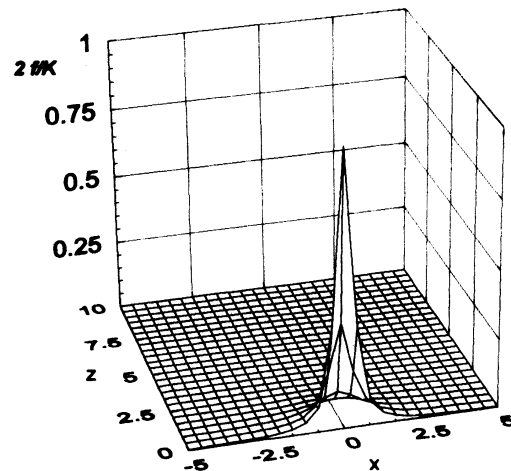Another important situation is the one characterized by a surface easy-axis distribution of the kind
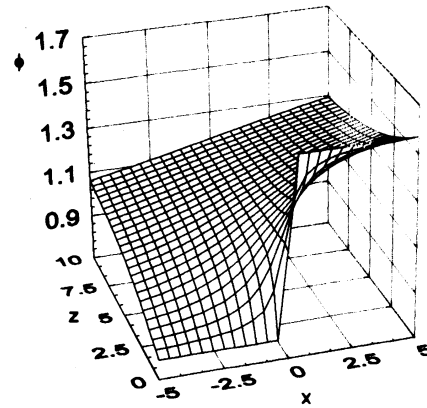
(a)
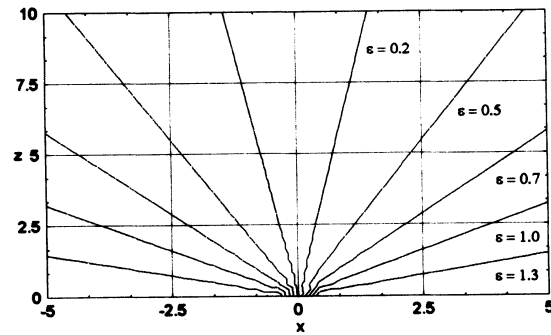
(b)

(c)

FIG. 1. Tilt angle distribution $\phi(x,z)$ [(a) and (b)] and energy density distribution (c) vs x and z. The nematic sample is approximated with a halfspace ($z > 0$). The easy-axis distribution is a step function of the kind $\Phi(x < 0) = \Phi_1$ and $\Phi(x > 0) = \Phi_2$. The anchoring energy is assumed infinite. (a) shows that an abrupt variation of $\phi(x,z)$ is localized near $x = 0$ for $z \to 0$. In the opposite limit of $z \to \infty$ the variation of $\phi(x,z)$ is smooth. (b) shows different "walls" for different ε parameters. (c) shows that the energy density of the tilt angle distribution for the considered case diverges for $(x,z) \to 0$, indicating that in the origin of our Cartesian reference frame is localized a dislocation.

$$\Phi(x) = \begin{cases} \Phi_1, & x < -\dfrac{\Lambda}{2} \\[2ex] \Phi_2, & -\dfrac{\Lambda}{2} < x < \dfrac{\Lambda}{2} \\[2ex] \Phi_1, & x > \dfrac{\Lambda}{2}. \end{cases} \qquad (8)$$

This situation refers to a surface nearly homogeneous, the easy axis forming the angle Φ_1 with the z axis and presenting a nonhomogeneity of thickness Λ, whose easy axis is Φ_2. In this case, Eq. (5) gives

$$\phi(x,z) = \Phi_1 + \frac{(\Phi_2 - \Phi_1)}{\pi} \left\{ \arctan\left[\frac{\dfrac{\Lambda}{2} + x}{z} \right] \right.$$
$$\left. + \arctan\left[\frac{\dfrac{\Lambda}{2} - x}{z} \right] \right\}. \qquad (9)$$

Very far from the surface (i.e., for $z \to \infty$), $\phi(x,z) \to \Phi_1$. Now the surface thickness of the wall of the nematic orientation is Λ, and it tends to zero very far from the orientating surface. $\phi(x,z)$ given by (9) is shown in Fig. 2(a). We can now apply the criterion introduced before to define the wall. It is now the region in which $\phi(x,z)$ strongly differs from Φ_1. By using Eq. (9), the border of the wall is defined by

$$\frac{\Phi_2 - \Phi_1}{\pi} \left\{ \arctan\left[\frac{\dfrac{\Lambda}{2} + x}{z} \right] + \arctan\left[\frac{\dfrac{\Lambda}{2} - x}{z} \right] \right\} = \varepsilon,$$

where ε has the same meaning as before. For $x > \dfrac{\Lambda}{2}$ this equation can be rewritten as

$$x^2 + \left[z - \frac{\dfrac{\Lambda}{2}}{\tan\left[\dfrac{\pi\varepsilon}{\Phi_2 - \Phi_1} \right]} \right]^2 = \left[\frac{\dfrac{\Lambda}{2}}{\sin\left[\dfrac{\pi\varepsilon}{\Phi_2 - \Phi_1} \right]} \right]^2.$$

A similar equation is obtained for $x < -\Lambda/2$. This relation shows that the border of the wall is a circle of radius

$$\Lambda/2 \csc[\pi\varepsilon/(\Phi_2 - \Phi_1)],$$

whose center is localized in

$$(0, \Lambda/2 \cot[\pi\varepsilon/\Phi_2 - \Phi_1]).$$

In Fig. 2(b) different walls corresponding to different ε's are shown.

The elastic energy density for the distortion given by (9) is

$$f = \tfrac{1}{2} K \left[\frac{\Phi_2 - \Phi_1}{\pi} \right]^2 \frac{\Lambda^2}{R_+^2 R_-^2}, \qquad (10)$$
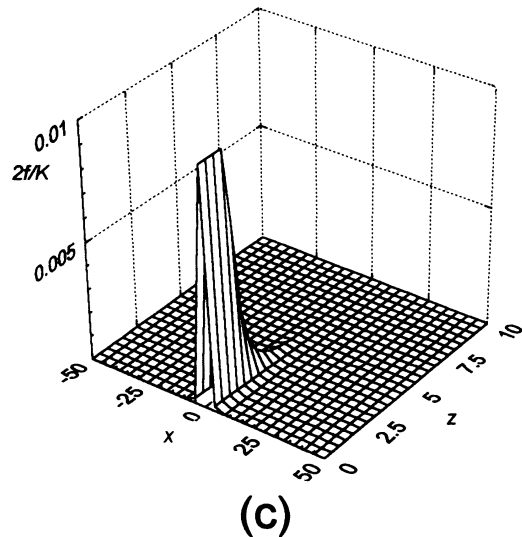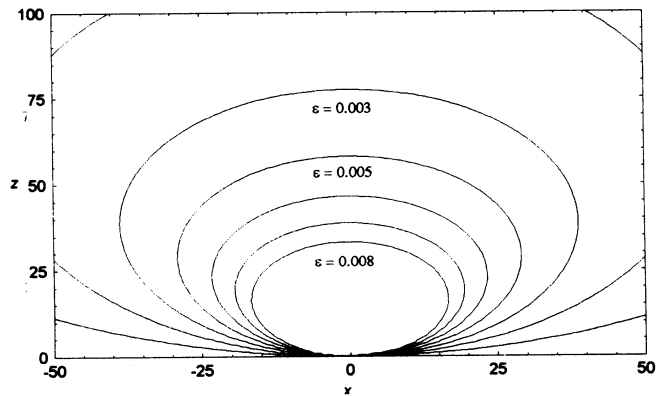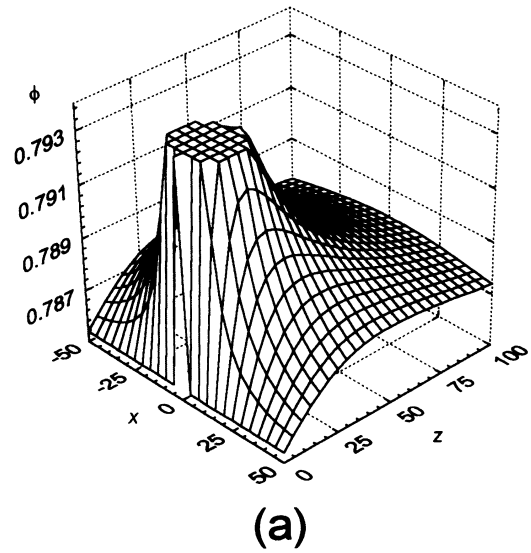

(a)

(b)

(c)

FIG. 2. As in Fig. 1 with the easy-axis distribution $\Phi(x) = \Phi_1$, $|x| > \Lambda/2$ and $\Phi(x) = \Phi_2$, $|x| < \Lambda/2$. (a) shows that $\phi(x,z)$ changes very much near $x = \pm\Lambda/2$ and $z \to 0$. In the opposite limit of $z \to \infty$, $\phi(x,z) \to \Phi_1$. (b) shows the border of the wall of orientation for different ε parameters. (c) gives the trend of the elastic energy density. It diverges for $x = \pm\Lambda/2$ and $z = 0$ and tends to zero for large z. In this case, in $(\pm\Lambda/2, 0)$ are present two dislocations. x and z are given in units of Λ.

where $R_{\pm}^2 = z^2 + (x \pm \Lambda/2)^2$. There are now two disclinations localized in $(\pm\Lambda/2, 0)$. The elastic energy density is proportional to $(\Phi_2 - \Phi_1)^2$ and Λ^2. The trend of f vs x and z is shown in Fig. 2(c), from which the position of the dislocation is clearly visible, coinciding with the divergent points of f.

A final situation that has some physical relevance is the one in which the surface tilt angle passes continuously from Φ_1 (at $x \to -\infty$) to Φ_2 (at $x \to +\infty$). A simple profile is

$$\Phi(x) = \begin{cases} \Phi_1, & x < -\dfrac{\Lambda}{2} \\[2mm] \Phi_m + \Delta \dfrac{x}{\Lambda}, & -\dfrac{\Lambda}{2} < x < \dfrac{\Lambda}{2} \\[2mm] \Phi_2, & x > \dfrac{\Lambda}{2}, \end{cases} \qquad (11)$$

where $\Phi_m = \frac{1}{2}(\Phi_1 + \Phi_2)$ and $\Delta = \Phi_2 - \Phi_1$. For this case Eq. (5) gives

$$\phi(x,z) = \tfrac{1}{2}(\Phi_1 + \Phi_2) + \frac{\Delta}{\pi}\left\{ \left[\frac{1}{2} + \frac{x}{\Lambda}\right]\arctan\left[\frac{\frac{\Lambda}{2} + x}{z}\right] - \left[\frac{1}{2} - \frac{x}{\Lambda}\right]\arctan\left[\frac{\frac{\Lambda}{2} - x}{z}\right] + \frac{3}{2\Lambda}\ln\left[\frac{z^2 + \left[\frac{\Lambda}{2} - x\right]^2}{z^2 + \left[\frac{\Lambda}{2} + x\right]^2}\right]\right\}. \qquad (12)$$

The thickness of the wall of orientation is Λ on the orienting surface and tends to infinity for $z \to \infty$, as in the case for which the surface orientation is given by (1).

The case considered now gives us the opportunity to extend to the weak-anchoring case the results obtained above. In this situation the total elastic energy per unit length along the y axis is given by

$$F = \int_{-\infty}^{\infty}\int_0^{\infty} \tfrac{1}{2}K(\nabla_\phi)^2 dx\, dz$$
$$+ \int_{-\infty}^{\infty} \tfrac{1}{2}W[\phi(x,0) - \Phi(x)]^2 dx \qquad (13)$$

in the above mentioned one-constant approximation. In (13) the second term takes into account the finite anchoring energy. It is written in the Rapini-Papoular form [26]. In it, $\phi(x,0)$ is the actual surface tilt angle, whereas $\Phi(x)$ is the easy axis. The minimization of (13) gives now again Eq. (4) for the bulk, i.e., for $-\infty < x < \infty$, $0 < z < \infty$, with the boundary condition

$$-K\left[\frac{\partial\phi}{\partial z}\right]_{z=0} + W[\phi(x,0) - \Phi(x)] = 0. \qquad (14)$$

Equation (14) is usually rewritten by introducing the extrapolation length $L = K/W$:

$$\phi(x,0) - \Phi(x) = L\left[\frac{\partial\phi}{\partial z}\right]_{z=0}. \qquad (15)$$

By taking into account that in this situation the actual surface angle is $\phi(x,0)$, Eq. (5) has to be rewritten as

$$\phi(x,z) = \frac{1}{\pi}\int_{-\infty}^{\infty}\frac{z}{z^2 + (x'-x)^2}\phi(x',0)dx'. \qquad (16)$$

By means of (16) the boundary condition (15) is written as

$$\phi(x,0) = \Phi(x) + \frac{L}{\pi}\int_{-\infty}^{\infty}\frac{\phi(x',0)dx'}{(x'-x)^2}. \qquad (17)$$

Equation (17), by observing that $(x'-x)^{-2} = -d(x'-x)^{-1}/dx'$, can be put in the form

$$\phi(x,0) = \Phi(x) + \frac{L}{\pi}\int_{-\infty}^{\infty}\frac{1}{x'-x}\frac{d\phi(x',0)}{dx'}dx'. \qquad (18)$$

Equations (17) or (18) are Freedholm equations of second kind. In the hypothesis in which L is a small quantity, they can be solved in an approximated manner, giving

$$\phi(x,0) = \Phi(x) + \frac{L}{\pi}\int_{-\infty}^{\infty}\frac{1}{x'-x}\frac{d\Phi(x')}{dx'}dx', \qquad (19)$$

at the first order in L. Of course, expression (19) is valid only for

$$\varepsilon(x) = \frac{L}{\pi}\int_{-\infty}^{\infty}\frac{1}{x'-x}\frac{d\Phi(x')}{dx'}dx' < 1, \qquad (20)$$

since the second term of (19) is a small perturbation to the first order solution. We can use Eq. (19) for the case in which the distribution of the surface easy axes is given by (11). By substituting (11) into (18), simple calculations give

$$\varepsilon(x) = \frac{\Delta L}{\pi\Lambda}\ln\left|\frac{x - \dfrac{\Lambda}{2}}{x + \dfrac{\Lambda}{2}}\right|. \qquad (21)$$

$\varepsilon(x)$ given by (21) represents the correction to $\Phi(x)$, the easy axis. Hence, in the regions in which (20) holds, the actual surface tilt angle is $\Phi(x) + \varepsilon(x)$. We observe that condition (20) gives, by using (21),

$$x_p \sim \frac{\Lambda}{2}\coth\left[\frac{\pi}{2\Delta}\frac{\Lambda}{L}\right], \qquad (22)$$

for $x > \Lambda/2$. The quantity $2x_p$ may be interpreted as the thickness of the surface wall of orientation. From (22) we derive that

$$x_p \to \frac{\Delta}{\pi}L \quad \text{for } \Lambda \to 0, \qquad (23)$$

which corresponds to the situation characterized by the

surface distribution of easy axes given by (1). Equation (23) states that in this case the thickness of the surface wall of orientation is of the order of the extrapolation length, as expected with a naive analysis of the problem. The result (23) may be also derived directly from Eq. (20), taking into account that (1) may be rewritten as

$$\Phi(x) = \Phi_1 + \Delta E(x) , \qquad (24)$$

where $E(x) = 0$ for $x < 0$ and 1, for $x > 0$ is the Heaviside step function. In this case, $dE(x)/dx = \delta(x)$, where $\delta(x)$ is the Dirac's delta function and Eq. (20) gives immediately (23). Another interesting physical limit is $L \to 0$, which corresponds to strong anchoring. In this case, Eq. (22) gives

$$x_p \to \frac{\Lambda}{2} ,$$

i.e., the thickness of the surface wall coincides with the region in which $\Phi(x)$ changes. The same kind of calculation can be performed for the case in which $\Phi(x)$ is given by (8). Following step by step the above procedure, one obtains

$$\varepsilon(x) = -\frac{\Delta L}{\pi} \frac{\Lambda}{\left[\dfrac{\Lambda}{2} + x\right]\left[\dfrac{\Lambda}{2} - x\right]} . \qquad (25)$$

The condition (20) gives now

$$x_p = \frac{\Lambda}{2}\left[1 + 4\frac{\Delta L}{\pi\Lambda}\right]^{1/2} , \qquad (26)$$

which in the $L/\Lambda < 1$ limit is equivalent to

$$x_p = \frac{\Lambda}{2} + \frac{\Delta L}{\pi} , \qquad (27)$$

i.e., the thickness of the surface wall is the one corresponding to the strong-anchoring situation plus a quantity of the order of the extrapolation length.

By following the previous procedure it is possible now to consider the case in which $\Phi(x)$ is given by (8), but the anchoring energy, whose extrapolation length is L, is finite. By means of Eq. (15) or Eq. (19), one derives

$$\varepsilon(x) = -\frac{(\Phi_2 - \Phi_1)}{\pi} \frac{L\Lambda}{\left[\dfrac{\Lambda}{2}\right]^2 - x^2} \qquad (28)$$

for the variation of the surface tilt angle connected with the weak anchoring. The condition (20) now gives

$$x_p = \frac{\Lambda}{2} - \frac{1}{\pi}(\Phi_2 - \Phi_1)L \qquad (29)$$

is the hypothesis of $L/\Lambda < 1$, as supposed. The thickness of the surface wall is then

$$2x_p = \Lambda - \frac{2}{\pi}(\Phi_2 - \Phi_1)L , \qquad (30)$$

i.e., it is reduced by a quantity of the order of L. This result is physically meaningful: the homogeneous regions characterized by Φ_1 squeeze the inhomogeneous part

characterized by Φ_2.

In concluding this section, we stress that for a semi-infinite sample characterized by Φ_1 ($x < 0$) and by Φ_2 ($x > 0$) and strong anchoring, the thickness of the wall of orientation is zero on the surface and it tends to infinity far from the surface. On the contrary for the weak-anchoring situation, characterized by an extrapolation length L, the surface thickness of the wall is zero and it tends again to infinity far from the surface. In other physical situations having a surface wall of orientation imposed by the surface treatment, we have shown that the weak anchoring only modifies the surface thickness, increasing it by a quantity proportional to the extrapolation length. However, at infinity the thickness of the wall remains zero or infinite according to the surface treatment. Consequently, it seems important to us to extend the preceding calculations to a NLC sample having the shape of a slab.

III. WALLS OF ORIENTATION IN A SLAB OF THICKNESS d

In this section the analysis of Sec. II will be extended to a sample of thickness d. The total elastic energy per unit length along the y axis is now

$$F = \int_{-d/2}^{d/2} \int_{-\infty}^{\infty} \tfrac{1}{2} K(\nabla\phi)^2 dx\, dz , \qquad (31)$$

in the strong-anchoring case and in the one-constant approximation. By minimizing (31) one obtains again Eq. (4), which has to be solved with the boundary condition

$$\phi\left(x, \frac{d}{2}\right) = \Phi_+(x) , \quad \text{and} \quad \phi\left(x, -\frac{d}{2}\right) = \Phi_-(x) , \qquad (32)$$

where $\Phi_+(x)$ and $\Phi_-(x)$ are the easy axes on the upper and lower surfaces, respectively. In a previous paper, the general solution of Eq. (4) satisfying the boundary conditions (32) has been given in terms of Green's functions [25]. It is

$$\phi(x,z) = \int_{-\infty}^{+\infty} [G_+(x' - x, z)\Phi_+(x') + G_-(x' - x, z)\Phi_-(x')]dx' , \qquad (33)$$

where

$$G_\pm(x' - x, z) = \frac{1}{2d} \frac{\cos\left[\dfrac{\pi}{d}z\right]}{\cosh\left[\dfrac{\pi}{d}(x' - x)\right] \mp \sin\left[\dfrac{\pi z}{d}\right]} . \qquad (34)$$

Let us suppose that the problem under consideration is symmetric, i.e.,

$$\Phi_+(x) = \Phi_-(x) \ . \tag{35}$$

This implies, as is easily shown, that

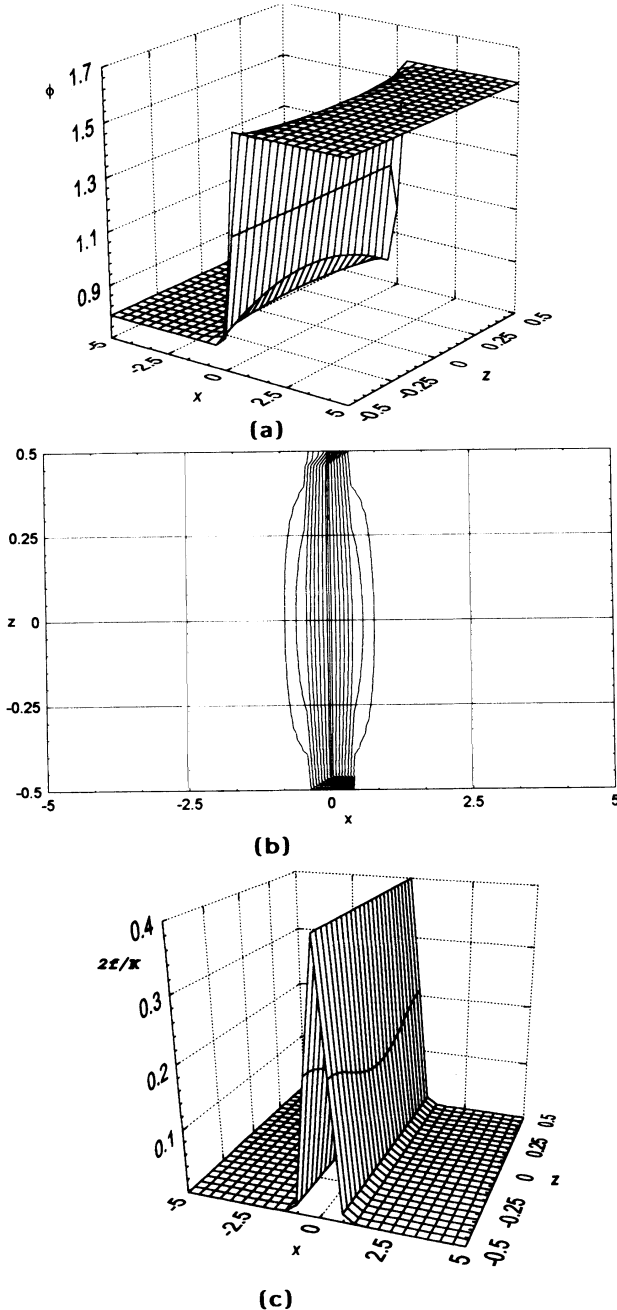$$\phi(x, -z) = \phi(x,z) \ . \tag{36}$$

(a)

(b)

(c)

FIG. 3. Tilt angle distribution $\phi(x,z)$ [(a) and (b)] and energy density distribution (c) vs x and z. The nematic sample is a slab of thickness d, characterized by the same easy-axis distribution of Fig. 1. The two surfaces are supposed to be exactly in phase (a). The variation of $\phi(x,z)$ is localized near $x=0$. The width of the wall of orientation is of the order of d, as shown in (b). The energy density diverges at $(0, \pm d/2)$, where two dislocation are localized (c). x and z are given in units of d.

In this case, Eq. (30) becomes

$$\phi(x,z) = \int_{-\infty}^{+\infty} [G_+(x'-x,z) + G_-(x'-x,z)] \Phi(x') dx' \ . \tag{37}$$

A simple inspection, by using (34), shows that

$$G_+(x'-x,-z) + G_-(x'-x,-z)$$
$$= G_+(x'-x,z) + G_-(x'-x,z) \ ,$$

as required. It is possible now to analyze the situation in which $\Phi(x)$ is of the same kind as (1). This refers to two identical surfaces characterized by a sharp variation of the easy axis and placed in an exact recorder. By substituting (1) in (37) one obtains for the tilt angle distribution in the NLC sample the expression

$$\phi(x,z) = \tfrac{1}{2}(\Phi_1 + \Phi_2)$$
$$+ \left[\frac{\Phi_2 - \Phi_1}{\pi} \right] \arctan \left[\frac{\sinh\left[\dfrac{\pi x}{d}\right]}{\cos\left[\dfrac{\pi z}{d}\right]} \right] \ , \tag{38}$$

which generalizes the previous Eq. (6) to a sample of finite thickness. Equation (38) shows that the thickness of the wall in surface is zero as a consequence of the strong-anchoring hypothesis. On the contrary, in the "bulk," i.e., in the middle of the sample (at $z=0$), the thickness of the wall is of the order of the thickness of the sample d. The trend of $\phi(x,z)$ given by (38) vs x and z is shown in Fig. 3(a). In Fig. 3(b) the wall of orientation is shown. By using (38), simple calculations give for the elastic energy density the expression

$$f = \tfrac{1}{2} K \left[\frac{\Phi_2 - \Phi_1}{d} \right]^2 \frac{1}{\cos^2\left[\dfrac{\pi z}{d}\right] + \sinh^2\left[\dfrac{\pi x}{d}\right]} \ , \tag{39}$$

which diverges for $z = \pm d/2$ and $x=0$, as expected, because in these two points two singularities are localized. f given by (39) is shown in Fig. 3(c). From this figure one derives that the energy density is mainly localized around the straight line $x=0$ presenting for $\pm d/2$ two divergent points.

Let us consider now the situation in which $\Phi(x)$ is given by (8). This case refers to two identical surfaces characterized by the easy axis Φ_1, presenting a nonhomogeneity of thickness Λ, exactly in phase. Now the general expression (37) gives
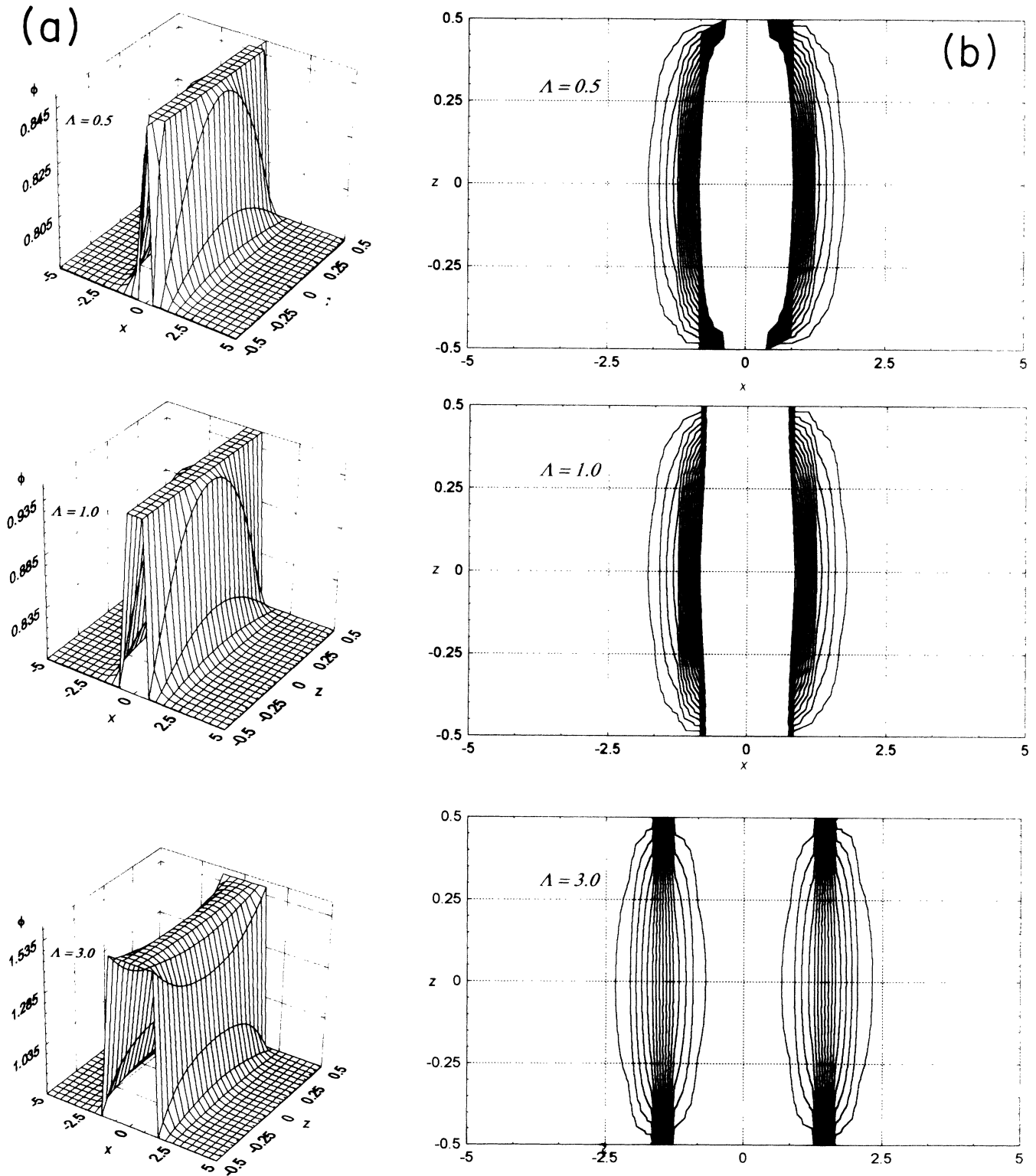
FIG. 4. The situation of Fig. 2 is extended to a nematic slab of thickness d formed by two identical surfaces exactly in phase. [(a) and (b)] refer to $\phi(x,z)$ vs x and z for different values of Λ. For $\Lambda < d$ there is a wall of orientation whose thickness, in the bulk, is of the order of $2d$ For $\Lambda > d$ there are two walls of orientation clearly separated. (c) shows the energy density. It diverges now in $(\pm\Lambda/2, \pm d/2)$, in which the dislocations are localized. x, z, and Λ are given in units of d.

$$\phi(x,z)=\Phi_1+\left[\frac{\Phi_2-\Phi_1}{\pi}\right]\left\{\arctan\left[\frac{\sinh\left[\frac{\pi}{d}\left[\frac{\Lambda}{2}+x\right]\right]}{\cos\left[\frac{\pi}{d}z\right]}\right]+\arctan\left[\frac{\sinh\left[\frac{\pi}{d}\left[\frac{\Lambda}{2}-x\right]\right]}{\cos\left[\frac{\pi z}{d}\right]}\right]\right\}. \tag{40}$$
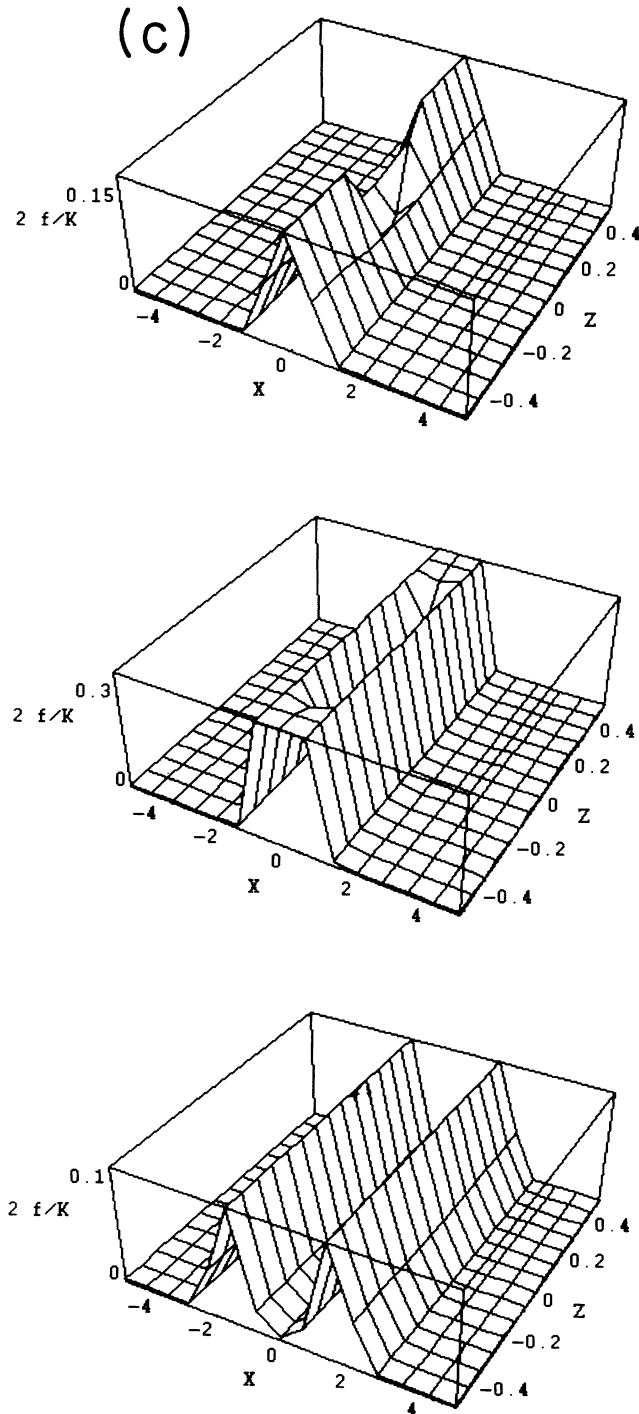
FIG. 4. (Continued).

It is important to note that the maximum value of $\phi(x,z)$ is reached for $x=z=0$. It is given by

$$\phi(0,0)=\Phi_1+2\frac{(\Phi_2-\Phi_1)}{\pi}\arctan\left[\frac{\pi\Lambda}{\sinh 2d}\right] . \tag{41}$$

It is of the order of Φ_2 only for $\Lambda \sim d$. For $\Lambda \ll d$ from (41) one obtains

$$\phi(0,0)=\Phi_1+(\Phi_2-\Phi_1)\frac{\Lambda}{d} , \quad \frac{\Lambda}{d}\ll 1 , \tag{42}$$

i.e., $\phi(0,0)$ strongly differs from Φ_2. The trend of $\phi(x,z)$ vs x and z for different Λ is shown in Fig. 4(a), whereas the walls of orientation are reported in Fig. 4(b). From this last figure one easily derives that the width of the wall of orientation is of the order of $\Lambda+2d$. In Fig. 4(c) the distribution of the elastic energy density for the same values of Λ is drawn. We underline that a better definition of the wall requires the analysis of the elastic energy density instead of the tilt angle distribution, because, in fact, this quantity strongly differs from zero in a well defined region that can be termed the "wall of distribution energy." A simple analysis shows that the two definitions of the wall of orientation are indeed equivalent, as expected.

A practical question arises: When is it possible experimentally to detect a wall of orientation of the kind described before? The optical experimental techniques are sensitive to the average of the square of the tilt angle, i.e., to

$$\langle[\phi(x,z)-\Phi_1]^2\rangle$$

$$=\frac{1}{ld}\int_{-l/2}^{l/2}\int_{-d/2}^{d/2}[\phi(x,z)-\Phi_1]^2dx\,dz , \tag{43}$$

where the x average is performed over l, which is connected with the diameter of the light beam. This average depends on $[\Phi_2-\Phi_1]^2$ and Λ and d as shown in Fig. 5. This figure shows that for $\Lambda>d$, $\langle[\phi(x,z)-\Phi_1]^2\rangle$ has a linear dependence with respect to Λ. However, for small Λ, $\langle[\phi(x,z)-\Phi_1]^2\rangle$ is nearly quadratic in Λ. In particular,

$$\{\partial\langle[\phi(x,z)-\Phi_1]^2\rangle/\partial\Lambda\}_{\Lambda=0}=0 .$$

Consequently, the optical experimental technique allows us to detect a wall of orientation only for Λ of the order of d. In the opposite limit it is very hard to visualize surface nonhomogeneities. This observation is important for the result that will be obtained in the next section, where
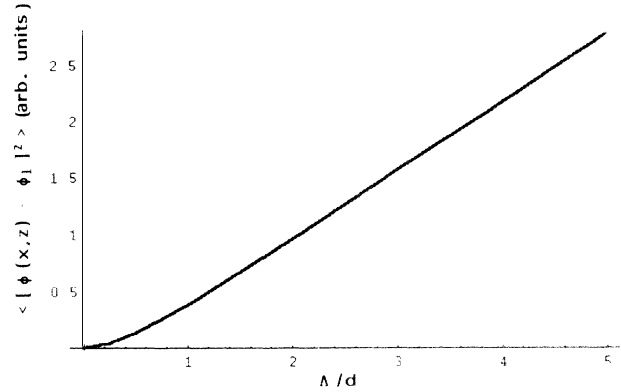

FIG. 5. Trend of detected birefringence of a sample presenting a surface nonhomogeneity of the kind $\Phi(x)=\Phi_2$, for $|x|<\Lambda/2$, and $\Phi(x)=\Phi_1$, for $|x|>\Lambda/2$. For $\Lambda>d$ the birefringence is proportional to Λ, whereas for $\Lambda<d$ it is nearly quadratic. The wall is easily detected only for $\Lambda>d$.

the Fréedericksz transition in nonhomogeneous surfaces will be analyzed.

We can now extend the preceding calculations to the weak-anchoring case. If we substitute Eq. (38) in Eq. (19), it is easy to find that

$$\varepsilon\left[x,\frac{d}{2}\right]=-\frac{(\Phi_2-\Phi_1)}{\pi}\frac{L}{\sinh\left[\frac{\pi x}{d}\right]} , \tag{44}$$

for the case in which the slab is characterized by surface tilt angles given by (1). The condition (20) gives

$$x_p\simeq\frac{\Phi_2-\Phi_1}{\pi}L . \tag{45}$$

Consequently, the thickness of the surface wall is

$$2x_p\simeq2\left|\frac{\Phi_2-\Phi_1}{\pi}\right|L , \tag{46}$$

i.e., of the order of the extrapolation length, independent of the thickness of the sample.

Let us consider, finally, the situation for which the surface tilt angles are given by (8). The same procedure followed above gives
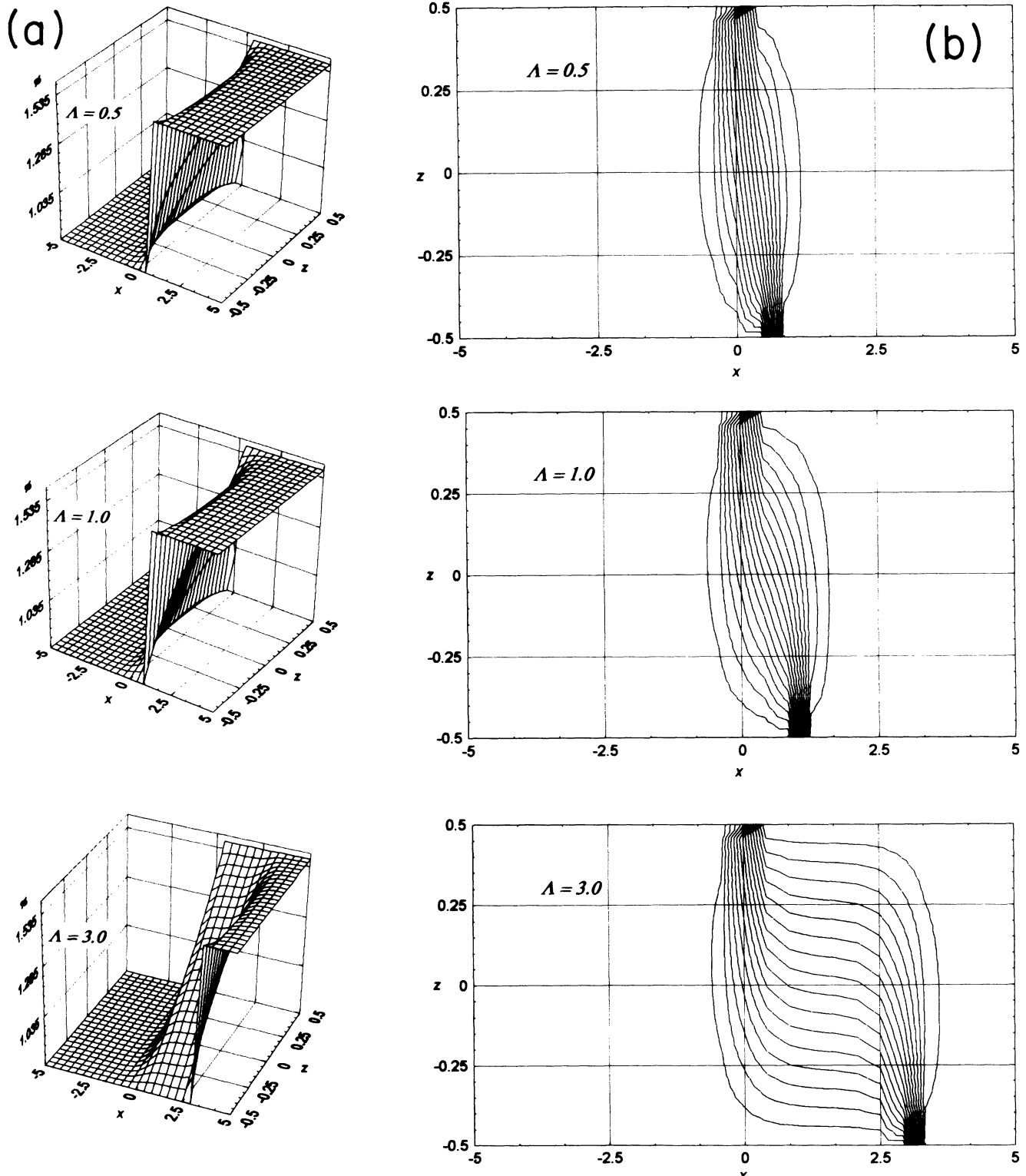
$$\varepsilon\left[x,\frac{d}{2}\right]=L\frac{\Phi_2-\Phi_1}{\pi}\frac{\sinh\left[\frac{\pi}{d}(\Lambda-x)\right]+\sinh\left[\frac{\pi}{d}(\Lambda+x)\right]}{\sinh\left[\frac{\pi}{d}(\Lambda-x)\right]\sinh\left[\frac{\pi}{d}(\Lambda+x)\right]} . \tag{47}$$

From Eq. (47) one derives for the thickness of the surface wall the expression

$$2x_p=\Lambda-2\left|\frac{\Phi_2-\Phi_1}{\pi}\right|L , \tag{48}$$

FIG. 6. As in Fig. 3, where the surfaces are out of phase of Λ. (a) is the $\phi(x,z)$ distribution and (b) is the wall of orientation. In the bulk its width is of the order of d. (c) is the energy density distribution diverging in $(0, -d/2)$ and $(\Lambda, d/2)$, in which the dislocations are located. The curves are drawn for different Λ. For Λ smaller than d, the width of the wall of orientation is of the order of the thickness of the sample. On the contrary, the $\Lambda > d$, the width is of the order of Λ. x, z, and Λ are given in units of d.

i.e., again the thickness of the surface wall is reduced by a quantity of the order of the extrapolation length.

The surfaces we have considered until now are equal and placed exactly in phase. It is possible to analyze briefly the case in which

$$\Phi_+(x)= \begin{cases} \Phi_1 , & x < \Lambda \\ \Phi_2 , & x > \Lambda \end{cases} \qquad \Phi_-(x)= \begin{cases} \Phi_1 , & x < 0 \\ \Phi_2 , & x > 0 , \end{cases} \tag{49}$$
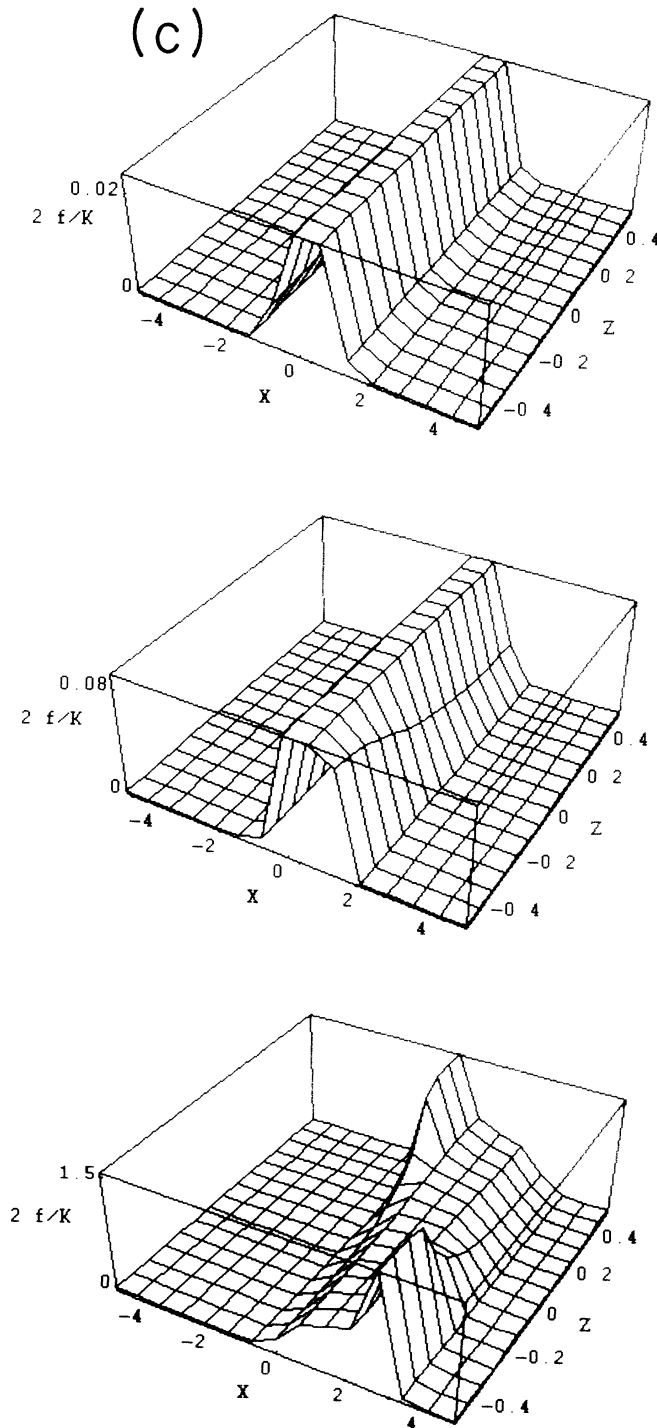

FIG. 6. (Continued).

relevant to two identical surfaces characterized by easy axes of the kind (1) displaced, one with respect to the other, by Λ. By using the general equation (33), one obtains for the tilt angle distribution,

$$\phi(x,z)=\tfrac{1}{2}(\Phi_1+\Phi_2)-\frac{(\Phi_2-\Phi_1)}{\pi}\arctan\frac{\left[1-\sin\left[\frac{\pi z}{d}\right]\right]\tanh\frac{\pi}{2d}(\Lambda-x)-\left[1+\sin\left[\frac{\pi z}{d}\right]\right]\tanh\frac{\pi x}{2d}}{\cos\left[\frac{\pi z}{d}\right]\left[1+\tanh\frac{\pi}{2d}(\Lambda-x)\tanh\frac{\pi x}{2d}\right]}$$

(50)

The trend of $\phi(x,z)$ vs x and z for different Λ is reported in Fig. 6(a). The delocalization of the orientation wall is shown in Fig. 6(b). For $\Lambda < d$, the thickness of the wall is of the order of d, whereas for Λ very large with respect to d it is of the order of $\Lambda + 2d$. Figure 6(c) exhibits the elastic energy density vs x and z for different values of the parameter Λ.

IV. FRÉEDERICKSZ TRANSITION FOR NONHOMOGENEOUS ANCHORING ENERGY

The Fréedericksz transition in a uniform sample is a well known effect described in many textbooks. It refers to a transition of orientation in NLC induced by an external field. In a particular situation of symmetry this transition of order is a second order phase transition for which the control parameter is the applied field and the order parameter the maximum value of the tilt angle [2–6]. The Fréedericksz transition has been analyzed in situations of strong and weak anchoring only for uniform samples. For a NLC slab of thickness d having easy direction parallel to the z axis (homeotropic alignment), submitted to an electric field parallel to the z axis, the threshold for the Fréedericksz effect is given by

$$E_{c\infty}=2\frac{\pi}{d}\left[\frac{\pi K}{-\varepsilon_a}\right]^{1/2},$$

(51)

in the strong-anchoring hypothesis, where K is the elastic constant and $\varepsilon_a=\varepsilon_\parallel-\varepsilon_\perp$ the dielectric anisotropy ($\parallel$ and $\perp$ refer to the NLC direction $\mathbf{n}$). For the considered experimental arrangement the Fréedericksz effect exists only for $\varepsilon_a < 0$.

In the case in which the anchoring energy is finite, the threshold is given by the Rapini-Papoular [26] expression

$$\frac{1}{\pi}\frac{d}{L}=\frac{E_c}{E_{c\infty}}\tan\left[\frac{\pi}{2}\frac{E_c}{E_{c\infty}}\right],$$

(52)

where L is the extrapolation length, E_c the actual field threshold, and $E_{c\infty}$ the threshold field for the strong-anchoring situation defined by (51).

The aim of this section is to generalize Eq. (52) for the situation in which $W=W(x)$ or $L=L(x)$, but the same on the two surfaces, i.e., $W_+(x)=W_-(x)$. When the NLC slab is submitted to an electric field parallel to z, the total energy per unit length along the y axis is given by

$$F=\int_{-\infty}^{\infty}\int_{-d/2}^{d/2}\left[\tfrac{1}{2}K(\nabla\phi)^2-\frac{\varepsilon_a}{8\pi}E^2\phi^2\right]dx\,dz$$

$$+\int_{-\infty}^{+\infty}\frac{1}{2}W_+(x)\phi^2\left[x,\frac{d}{2}\right]dx$$

$$+\int_{-\infty}^{+\infty}\frac{1}{2}W_-(x)\phi^2\left[x,-\frac{d}{2}\right]dx\,,$$

(53)

in the limit of small ϕ. Equation (53) is written by supposing that the easy axis is parallel to z, but the surfaces are assumed nonhomogeneous with respect to the anchoring energy. By minimizing (53) one obtains

$$\frac{\partial^2\phi}{\partial x^2}+\frac{\partial^2\phi}{\partial z^2}+\lambda^2\phi=0\,,\quad-\frac{d}{2}\leq z\leq\frac{d}{2}\,,\quad-\infty<x<\infty\,,$$

(54)

for the bulk, with the boundary condition

$$L_+(x)\left[\frac{\partial\phi}{\partial z}\right]_{z=\frac{d}{2}}+\phi\left[x,\frac{d}{2}\right]=0\,,$$

$$-L_-(x)\left[\frac{\partial\phi}{\partial z}\right]_{z=-\frac{d}{2}}+\phi\left[x,-\frac{d}{2}\right]=0\,.$$

(55)

In (54), $\lambda^2=(-\varepsilon_a/4\pi K)E^2$ is the inverse of the well known dielectric coherence length square [2–6].

It is possible to expand the solution of (54) in plane waves along the x axis as follows:

$$\phi(x,z)=\int_{-\infty}^{+\infty}h(k,z)e^{ikx}dk\,,$$

(56)

where $h(k,z)=h(-k,z)$, since $\phi(x,z)$ is a real quantity. By substituting (56) into (54) one obtains for $h(k,z)$ the expression

$$h(k,z)=\alpha(k)e^{\bar{k}z}+\beta(k)e^{-\bar{k}z}\,,$$

(57)

where

$$\bar{k}\equiv\sqrt{k^2-\lambda^2}\,,$$

(58)

and $\alpha(k)$ and $\beta(k)$ have to be determined by means of the boundary conditions (55). Calculations similar to those performed in Ref. [25] give, for the function $\phi(x,z)$ we are looking for, the expression

$$\phi(x,z)=\frac{1}{2\pi}\int_{-\infty}^{+\infty}dx'\left[\phi\left[x',\frac{d}{2}\right]g_1(x-x',z)\right.$$

$$\left.-\phi\left[x',-\frac{d}{2}\right]g_2(x-x',z)\right] , \tag{59}$$

where the new propagators $g_i(x-x',z)$ $(i=1,2)$ are given by

$$g_1(x-x',z)=\int_{-\infty}^{+\infty}\frac{\sinh\left[\bar{k}\left[z+\frac{d}{2}\right]\right]}{\sinh(\bar{k}d)}e^{ik(x-x')}dk ,$$

$$\tag{60}$$

$$g_2(x-x',z)=\int_{-\infty}^{+\infty}\frac{\sinh\left[\bar{k}\left[z-\frac{d}{2}\right]\right]}{\sinh(\bar{k}d)}e^{ik(x-x')}dk .$$

By substituting expression (59) into the boundary conditions (55), one has

$$\frac{L_+(x)}{2\pi}\int_{-\infty}^{\infty}dx'\left[\phi\left[x',\frac{d}{2}\right]g^{(+)}(x-x')-\phi\left[x',-\frac{d}{2}\right]g^{(-)}(x-x')\right]+\phi\left[x,\frac{d}{2}\right]=0 ,$$

$$-\frac{L_-(x)}{2\pi}\int_{-\infty}^{\infty}dx'\left\{\phi\left[x',\frac{d}{2}\right]g^{(-)}(x-x')-\phi\left[x',-\frac{d}{2}\right]g^{(+)}(x-x')\right\}+\phi\left[x,-\frac{d}{2}\right]=0 ,$$

$$\tag{61}$$

where

$$g^{(+)}(x-x')=\int_{-\infty}^{+\infty}e^{ik(x-x')}\bar{k}\frac{\cosh(\bar{k}d)}{\sinh(\bar{k}d)}dk , \tag{62a}$$

$$g^{(-)}(x-x')=\int_{-\infty}^{+\infty}e^{ik(x-x')}\frac{\bar{k}}{\sinh(\bar{k}d)}dk . \tag{62b}$$

The above equations [(54)–(62)] are general and constitute the basic theoretical tool to investigate the Fréedericksz effect in the weak-anchoring situation when the anchoring energy is nonuniform. In the particular case in which $W_+(x)=W_-(x)$ [i.e., $L_+(x)=L_-(x)$], implying $\phi(x,d/2)=\phi(x,-d/2)$ and hence $\phi(x,z)=\phi(x,-z)$, Eqs. (59) can be rewritten as

$$\phi(x,z)=\frac{1}{2\pi}\int_{-\infty}^{+\infty}dx'\phi\left[x,\frac{d}{2}\right]\{g_1(x-x',z)$$

$$-g_2(x-x',z)\} , \tag{63}$$

and the boundary conditions assume the form

$$\frac{L(x)}{2\pi}\int_{-\infty}^{+\infty}dx'\phi\left[x',\frac{d}{2}\right][g^{(+)}(x-x')-g^{(-)}(x-x')]$$

$$+\phi\left[x,\frac{d}{2}\right]=0 . \tag{64}$$

In this simple case, by means of Eq. (62), it is easy to conclude that

$$g^{(+)}(x-x')-g^{(-)}(x-x')$$

$$=-\int_{-\infty}^{+\infty}e^{ik(x-x')}\bar{k}\tanh\left[\frac{\bar{k}d}{2}\right]dk . \tag{65}$$

Equation (64) solves our problem. In the case in which $W_+(x)=W_-(x)=W$ is position independent, $\phi(x,d/2)$ is expected also to be x independent. In this situation, by taking into account that $\int_{-\infty}^{+\infty}e^{ik(x-x')}dx'=2\pi\delta(x-x')$,

Eq. (64) gives

$$L\lambda\cot\left[\frac{\lambda d}{2}\right]=1 , \tag{66}$$

which is equivalent to Eq. (52) written above. In the case in which (64) holds, we may rewrite it in the form

$$\phi\left[x,\frac{d}{2}\right]=\frac{L(x)}{2\pi}\int_{-\infty}^{+\infty}dx'\phi\left[x',\frac{d}{2}\right]$$

$$\times[g^{(-)}(x-x')-g^{(+)}(x-x')] , \tag{67}$$

which clearly shows that

$$g^{(-)}(x-x')-g^{(+)}(x-x')=\frac{2\pi}{L(x')}\delta(x-x') . \tag{68}$$

From this expression and expression (65), one obtains

$$\frac{2\pi}{L(x')}\delta(x-x')=-\int_{-\infty}^{+\infty}e^{ik(x-x')}\bar{k}\,tgh\left[\bar{k}\frac{d}{2}\right]dk . \tag{69}$$

By integrating (69) over x' and using the integral representation of the Dirac δ function, it is simple to deduce

$$L(x)\lambda\cot\frac{\lambda d}{2}=1 . \tag{70}$$

This equation states that the threshold is fixed by the minimum value of the anchoring energy. This result is *a posteriori* physically consistent with the definition of threshold in a sample characterized by weak-anchoring energy. Consequently, the true theoretical threshold for the Fréedericksz effect in a NLC sample having nonhomogeneous anchoring energy is fixed by the lowest value of this parameter. This fact may have important consequences for the experimental determination of the anchoring energy by means of the Fréedericksz effect. However, as we have seen in Sec. III, a surface orientation inhomogeneity is experimentally detectable only if

the region over which it appears is of the same order of the thickness of the sample. Consequently, only if the lowest anchoring energy appears over a region whose thickness is of the order of d, it may induce experimentalists to a wrong determination of W. Otherwise, the experimentalist measures a threshold that corresponds to an x average of this parameter. For λ larger than the threshold value, Eqs. (67) and (63) allow us to determine $\phi(x,z)$.

V. CONCLUSIONS

The wall of orientation induced by surface nonhomogeneities in NLC have been theoretically analyzed. In the case in which the NLC sample may be approximated as a semi-infinite medium, we have shown that the surface thickness of the wall coincides with the geometrical nonhomogeneity region in the strong-anchoring hypothesis. On the contrary, for weak-anchoring energy, the expected variation of the thickness of the wall is of the order of the thickness of the sample, slightly modified by the anchoring energy. The problem connected with the experimental determination of surface walls in real samples has been also discussed. The analysis shows that they are detectable only if the surface nonhomogeneity is delocalized over a region whose width is of the order of the sample thickness. The influence of surface *nonhomogeneities* of anchoring energy on the threshold of the Fréedericksz effect have been analyzed too. Its connection with the experimental determination of the anchoring energy measured in this manner is meaningful only if W is *nonhomogeneous* over a region smaller than the thickness of the sample.

[1] J. L. Ericksen, Adv. Liq. Cryst. **2**, 233 (1976).
[2] F. M. Leslie, *Theory and Applications of Liquid Crystals,* edited by J. L. Ericksen and D. Kinder Leher (Springer-Verlag, Berlin, 1987).
[3] P. G. de Gennes, *Physics of Liquid Crystals* (Oxford University Press, New York, 1974).
[4] S. Chandrasekhar, *Liquid Crystals* (Cambridge University Press, Cambridge, England, 1977).
[5] G. Vertogen and W. H. de Jeu, *Thermotropic Liquid Crystals, Fundamentals* (Springer Verlag, Berlin, 1988).
[6] E. B. Priestley, P. J. Wojtowicz, and Ping Sheng, *Introduction to Liquid Crystals* (Plenum, New York, 1977).
[7] V. Fréedericksz and V. Zolina, Z. Kristallogr. Kristallgeom. Kristallphys. Kristallchem. **79**, 225 (1931).
[8] E. Kaneko, *Liquid Crystal TV Display (Principles and Applications of Liquid Crystals Displays)* (KTK, Tokyo, 1986).
[9] G. Barbero, F. Simoni, and P. Aiello, J. Appl. Phys. **55**, 304 (1984).
[10] *Liquid Crystals: Applications and Uses,* edited by B. Badahur (World Scientific, Singapore, 1991), Vols. I–III.
[11] I. Dozov, Ph. Martinot-Lagarde, and G. Durand, J. Phys. (Paris) Lett. **43**, 365 (1982).
[12] I. Dozov, Ph. Martinot-Lagarde, and G. Durand, J. Phys. (Paris) Lett. **44**, 817 (1983).
[13] N. V. Madhusudana and G. Durand, J. Phys. (Paris) Lett.

46, 195 (1985).
[14] G. Barbero, N. V. Madhusudana, J. F. Palierne, and G. Durand, Phys. Lett. **103A**, 385 (1984).
[15] G. Barbero, N. V. Madhusudana, and G. Durand, Z. Naturforsch. Teil A **37**, 1066 (1984).
[16] C. Oldano, Phys. Rev. Lett. **56**, 1098 (1984).
[17] E. Miraldi, C. Oldano, and A. Strigazzi, Phys. Rev. A **34**, 4348 (1986).
[18] G. Barbero, E. Miraldi, and C. Oldano, Phys. Rev. A **38**, 519 (1988).
[19] U. D. Kini, J. Phys. (Paris) **47**, 693 (1986); **47**, 1829 (1986); **48**, 1187 (1987).
[20] M. Zenginoglou, J. Phys. (Paris) **48**, 1599 (1987).
[21] F. Lonberg and R. B. Meyer, Phys. Rev. Lett. **55**, 718 (1985).
[22] M. Kléman, *Points, Lignes, Parois* (Editions de Physique Les Ulis, Orsay, 1977).
[23] H. L. Ong, A. J. Hurd, and R. B. Meyer, J. Appl. Phys. **57**, 186 (1985).
[24] G. Barbero, T. Beica, A. L. Alexe-Ionescu, and R. Moldovan, J. Phys. (France) II, **2**, 2011 (1982).
[25] L. R. Evangelista and G. Barbero, Phys. Rev. E **48**, 1163 (1993).
[26] A. Rapini and M. Papoular, J. Phys. (Paris) Colloq. **30**, 04 (1969).